Structural optimization and segregation behavior of quaternary alloy nanoparticles based on simulated annealing algorithm*

Xin-Ze Lu(陆欣泽)[1], Gui-Fang Shao(邵桂芳)[2,†], Liang-You Xu(许两有)[2], Tun-Dong Liu(刘暾东)[2], and Yu-Hua Wen(文玉华)[1]

[1] *Department of Physics, Xiamen University, Xiamen* 361005, *China*
[2] *Department of Automation, Xiamen University, Xiamen* 361005, *China*

(Received 9 December 2015; revised manuscript received 7 January 2016; published online 1 April 2016)

Alloy nanoparticles exhibit higher catalytic activity than monometallic nanoparticles, and their stable structures are of importance to their applications. We employ the simulated annealing algorithm to systematically explore the stable structure and segregation behavior of tetrahexahedral Pt–Pd–Cu–Au quaternary alloy nanoparticles. Three alloy nanoparticles consisting of 443 atoms, 1417 atoms, and 3285 atoms are considered and compared. The preferred positions of atoms in the nanoparticles are analyzed. The simulation results reveal that Cu and Au atoms tend to occupy the surface, Pt atoms preferentially occupy the middle layers, and Pd atoms tend to segregate to the inner layers. Furthermore, Au atoms present stronger surface segregation than Cu ones. This study provides a fundamental understanding on the structural features and segregation phenomena of multi-metallic nanoparticles.

Keywords: alloy nanoparticle, simulated annealing algorithm, structural stability, segregation

PACS: 36.40.–c, 61.46.Df, 52.65.Pp **DOI:** 10.1088/1674-1056/25/5/053601

1. Introduction

Metallic nanoparticles (NPs) are extensively used in chemical industry, petroleum industry, new energy, and environmental protection (such as air purification and sewage treatment).[1,2] Among these NPs, noble metal NPs have attracted much attention due to their excellent catalytic activity and good stability. For example, the available experimental and theoretical studies reveal that platinum (Pt) NPs are excellent and versatile catalysts in various important reactions. In particular, bi- or multi-metallic NPs can make full use of the synergy effects of crystal structures and electronic structures of these metals when Pt alloys with other kinds of metals. Accordingly, the alloy NPs may exhibit higher catalytic activity and selectivity compared with the monometallic ones.[3]

In recent years, most research has focused on bimetallic NPs, such as Pt–Au, Pt–Pd, and Pt–Cu.[4–8] Nowadays, trimetallic NPs also receive more and more attention.[9–14] However, the quaternary alloy NPs have rarely been studied. The available research only focuses on the experimental preparation of the NPs rather than their structures and stability.[15–17] In the study of the structural stability of NPs, the fundamental method is to calculate the total energy of the system and thereby to predict its stable structures. However, the potential energy surface of NPs is a three-dimensional curved surface. Therefore, the essence of the NP structure optimization is to search the global minimum point (corresponding to the lowest-energy structure) on the three-dimensional energy surface. In addition, the potential energy surface in the three-dimensional space is rugged, and the locally optimal number of potential energy functions grows rapidly as the NP size grows. Thus, the structural optimization of NPs actually belongs to a non-deterministic polynomial problem. The most effective way to solve this problem is to develop a more efficient and more precise global optimization algorithm.

Currently, several theoretical methods, such as molecular dynamic methods, Monte Carlo methods, and density functional theory (DFT) calculations, have been used to explore the stable structures of alloy NPs. The traditional Monte Carlo methods easily drop into a local optimum in the structural optimization of NPs,[18–22] therefore it is difficult to find the global optimum. To effectively predict the structural properties of NPs, more intelligent evolutionary algorithms such as the genetic algorithm and the particle swarm optimization (PSO) method[23–26] have been introduced. For example, the genetic algorithms have been used to study the stable structures of Pd–Au bimetallic NPs.[23–25] Chen proposed a spherical cut-cross genetic evolution to predict the clusters' structure.[26] In our previous study, the Monte Carlo methods were introduced to predict the stable structure of Pt–Pd bimetallic NPs by changing the exchange sequence.[27] However, there are some uncertainties, such as the operator selection and parameter setting, existing in these random intelligent optimization methods. It is crucial to search for high efficiency algorithms for the structural optimization of NPs.

*Project supported by the National Natural Science Foundation of China (Grant Nos. 51271156, 11474234, and 61403318) and the Natural Science Foundation of Fujian Province of China (Grant Nos. 2013J01255 and 2013J06002).

†Corresponding author. E-mail: gfshao@xmu.edu.cn

© 2016 Chinese Physical Society and IOP Publishing Ltd

In this paper, we will employ the simulated annealing (SA) algorithm to explore the stable structure of Pt–Pd–Cu–Au alloy NPs. The surface segregation behavior of the NPs is investigated by analyzing the atomic distribution, the radial distribution function, and the distribution of atomic coordination number. Further, we discuss the relationship between the atomic distributions and the compositions of the NPs.

2. Methods

2.1. The Q-SC many-body potentials

In this paper, the interatomic interaction in Pt–Pd–Cu–Au quaternary alloy NPs is described by the quantum corrected Sutton–Chen (Q-SC) many-body potentials. According to the Q-SC force field, the total potential energy of the system is expressed as

$$U = \sum_i U_i = \sum_i \varepsilon \left[\frac{1}{2} \sum_{j \neq i} V(R_{ij}) - c\sqrt{\rho_i} \right], \tag{1}$$

where R_{ij} is the distance between atoms i and j, ε is the energy scale factor, $V(R_{ij})$ is a pair interaction function defined by

$$V(R_{ij}) = \left(\frac{a}{R_{ij}} \right)^n, \tag{2}$$

and ρ_i is a local electron density accounting for cohesion associated with atom i defined by the following equation:

$$\rho_i = \sum_{j \neq i} \left(\frac{a}{R_{ij}} \right)^m. \tag{3}$$

In Eqs. (1)–(3), a is the length parameter, c is a dimensionless parameter, and n and m are integer parameters that satisfy the constraint $n > m$.[28–30] The model parameters for Pt, Pd, Cu, and Au are listed in Table 1.

Table 1. Potential parameters for Pt–Pd–Cu–Au NPs.[31]

Element	n	m	ε/meV	c	a/Å
Pt	11	7	9.7894	71.336	3.9163
Pd	12	6	3.2864	148.205	3.8813
Cu	10	5	5.7921	84.843	3.6030
Au	11	8	7.8052	53.581	4.0651

For describing the interatomic interaction between different metals, the geometric mean is used to obtain the energy parameter ε, while the arithmetic mean is used for the remaining parameters.[5,27]

2.2. The initial configuration

To conduct the atomistic simulation, tetrahexahedral (THH) NPs,[32] covered by high-index facets, are chosen as the initial atomic configuration. Firstly, a large face-centered cubic (fcc) single crystal is created. Subsequently, a square pyramid is used to cap this cube on each face along the direction of the crystal. Finally, THH NPs bounded by 24 {210} facets are obtained. Furthermore, Pt and other metallic atoms (Pd, Cu, and Au) are randomly distributed in the THH NPs by computer-produced random seeds. Figure 1 shows the illustration of THH NPs.

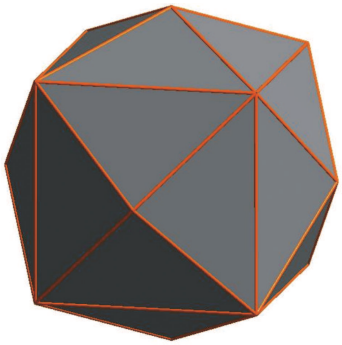


Fig. 1. (color online) Schematic illustration of THH NPs.

2.3. The optimization model

Generally, the most stable structure of NPs corresponds to the lowest-energy structure. Therefore, we can transfer the structural optimization of NPs into searching for their lowest-energy structures.

For Pt–Pd–Cu–Au quaternary alloy NP consisting of N atoms, let w_0, w_1, w_2, and w_3 denote the proportions of the four types of atoms (element 1, element 2, element 3, and element 4, respectively) and $w_0 + w_1 + w_2 + w_3 = 1$. Subsequently, arabic numerals are used to code different types of atoms, where 0, 1, 2, and 3 represent element 1, element 2, element 3, and element 4, respectively. Therefore, we can define a combinational optimization model for Pt–Pd–Cu–Au NPs as follows:

$$f_{\text{tot}} = \sum_{i=1}^{N} \varepsilon \left[\sum_{j=1, j \neq i}^{N} \frac{1}{2} V(R_{ij}) - c\sqrt{\rho_i} \right]. \tag{4}$$

The parameters m, n, a, and ε are calculated according to the following method. Firstly, let λ be the type of atom i and μ be the type of atom j ($\lambda = 0, 1, 2, 3$ and $\mu = 0, 1, 2, 3$). Let an identity matrix be

$$\boldsymbol{E} = [\boldsymbol{e}_0, \boldsymbol{e}_1, \boldsymbol{e}_2, \boldsymbol{e}_3] = \begin{bmatrix} 1 & 0 & 0 & 0 \\ 0 & 1 & 0 & 0 \\ 0 & 0 & 1 & 0 \\ 0 & 0 & 0 & 1 \end{bmatrix},$$

$$\boldsymbol{e}_0 = \begin{bmatrix} 1 \\ 0 \\ 0 \\ 0 \end{bmatrix}, \quad \boldsymbol{e}_1 = \begin{bmatrix} 0 \\ 1 \\ 0 \\ 0 \end{bmatrix}, \quad \boldsymbol{e}_2 = \begin{bmatrix} 0 \\ 0 \\ 1 \\ 0 \end{bmatrix}, \quad \boldsymbol{e}_3 = \begin{bmatrix} 0 \\ 0 \\ 0 \\ 1 \end{bmatrix}. \tag{5}$$

A symmetric matrix is given by

$$\boldsymbol{P} = \begin{bmatrix} p_{00} & p_{01} & p_{02} & p_{03} \\ p_{10} & p_{11} & p_{12} & p_{13} \\ p_{20} & p_{21} & p_{22} & p_{23} \\ p_{30} & p_{31} & p_{32} & p_{33} \end{bmatrix}. \tag{6}$$

Then we can describe the interaction between atom i and atom j as $p_{ij} = \boldsymbol{e}_\lambda^{\mathrm{T}} \boldsymbol{P} \boldsymbol{e}_\mu$, $p = \{m,n,a,\varepsilon\}$, which can be alternately calculated as follows:

$$\begin{aligned} &p_{\lambda\mu} = \frac{1}{2}(p_\lambda + p_\mu), \\ &p = \{m,n,a\}, \quad \lambda = 0,1,2,3, \quad \mu = 0,1,2,3, \\ &\varepsilon_{\lambda\mu} = \sqrt{\varepsilon_\lambda \varepsilon_\mu}. \end{aligned} \tag{7}$$

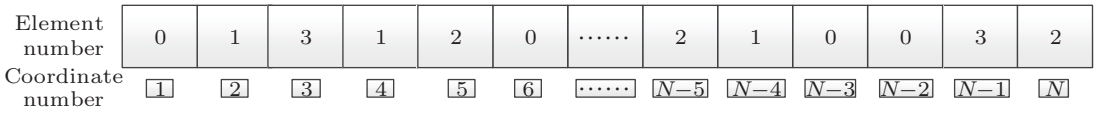
The c_i is determined by the equilibrium lattice parameter.

2.4. The SA algorithm

The earliest idea of SA algorithm was proposed by Metropolis *et al.* in 1953.[33] In 1983, Kirkpatrick and co-authors successfully introduced the annealing thought to the combinatorial optimization field.[34] Annealing thought is a kind of stochastic optimization algorithm based on the Monte–Carlo iterative solution strategy. The starting point for annealing thought is based on the similarity between the annealing processes of a material in physics and the general combinatorial optimization problem. The SA algorithm starts from a high initial temperature. As the temperature decreases, it may search for the objective function's global optimum in solution space. So far, the SA algorithm has achieved great success in combinatorial optimization, production scheduling, machine learning, circuit design, neural network, and other fields.

2.5. Coding

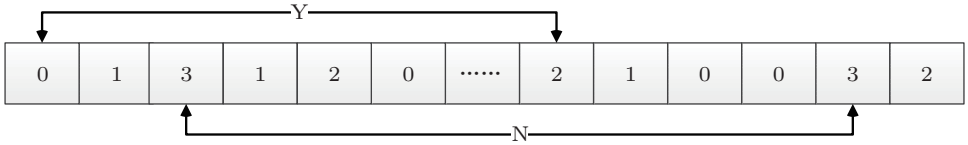
The structural optimization of NPs belongs to a discrete problem. Therefore, we use an integer coding method. For an NP with N atoms, let w_1, w_2, w_3, w_4 denote the proportions of four types of atoms, respectively, and $w_1 + w_2 + w_3 + w_4$=1. Use numbers 0, 1, 2, and 3 to represent the Pt, Pd, Cu, and Au atoms, respectively. All the coordinates of atoms in the NP are numbered from 1 to N. The coding scheme is defined as follows:



The corresponding numbers of the four types of atoms are $p_0 = N \times w_0$, $p_1 = N \times w_1$, $p_2 = N \times w_2$, and $p_3 = N \times w_3$. Each sequence of 0, 2, 2, and 3 represents a solution of the problem in the solution space, and it also represents a structure of the Pt–Pd–Cu–Au quaternary NP. To construct an initial feasible solution, various atoms are randomly distributed in the N coordinate space subject to the above constraints.

2.6. Neighborhood searching

Through continuous searching iteration, a neighborhood searching makes further adjustments to the feasible solution so as to approach an optimal solution. In this paper, we use the SA algorithm for neighborhood construction. With a feasible solution with N atoms, we randomly exchange two atoms' positions to generate new solutions and calculate the corresponding fitness. To avoid useless searches, two exchanged atoms must be different types. As shown below, atom 0 and atom 2 exchange will result in a new explanation, and this exchange is effective. However, when atom 3 exchanges with another atom 3, there is no change to the current solution, so this exchange is invalid.



There are ρ ($\rho = \rho_0\rho_1\rho_2\rho_3$) solutions for each state. As the particle size increases, the neighborhood solutions grow exponentially. However, we change only a pair of atoms each time. During the late stage of the search, the optimization speed is slow. Therefore, for the larger size NP, we make the following improvements.

In the SA search process, according to the search generation and cluster size, we determine a sequence position parameter for each search. Early in the search, to accelerate the optimization progress, each of the variable parameters is assigned a larger progressively decreasing constant K. To obtain the optimal result, iterations are terminated when K reaches 1. In this paper, the setting of K is as follows:

$$K = \begin{cases} \left\lfloor \dfrac{N_{\mathrm{o}}}{200}\left(1 - \dfrac{i}{0.8 i_{\max}}\right) \right\rfloor, & i < 0.8 i_{\max}, \\ 1, & i \geq 0.8 i_{\max}, \end{cases} \tag{8}$$

where N_{o} is the optimal size of the clusters (i.e., the number of atoms in the clusters), $i_{\max}$ is the largest search generation, and i is the current search generation.

2.7. Judgement

In the SA algorithm, we choose the Q-SC potential function as the fitness function. When the algorithm runs, the current solution is updated if we find a lower energy than the en-

ergy of the current solution. If the mutated energy is higher than the current solution's energy, the new solution is accepted based on a probability calculated as follows:

$$P = \exp(-\Delta E/Tk_0), \tag{9}$$

where ΔE is the particle energy difference between the new solution and the current solution; k_0 is the temperate change rate (generally between 0–1); and T is the current temperature.

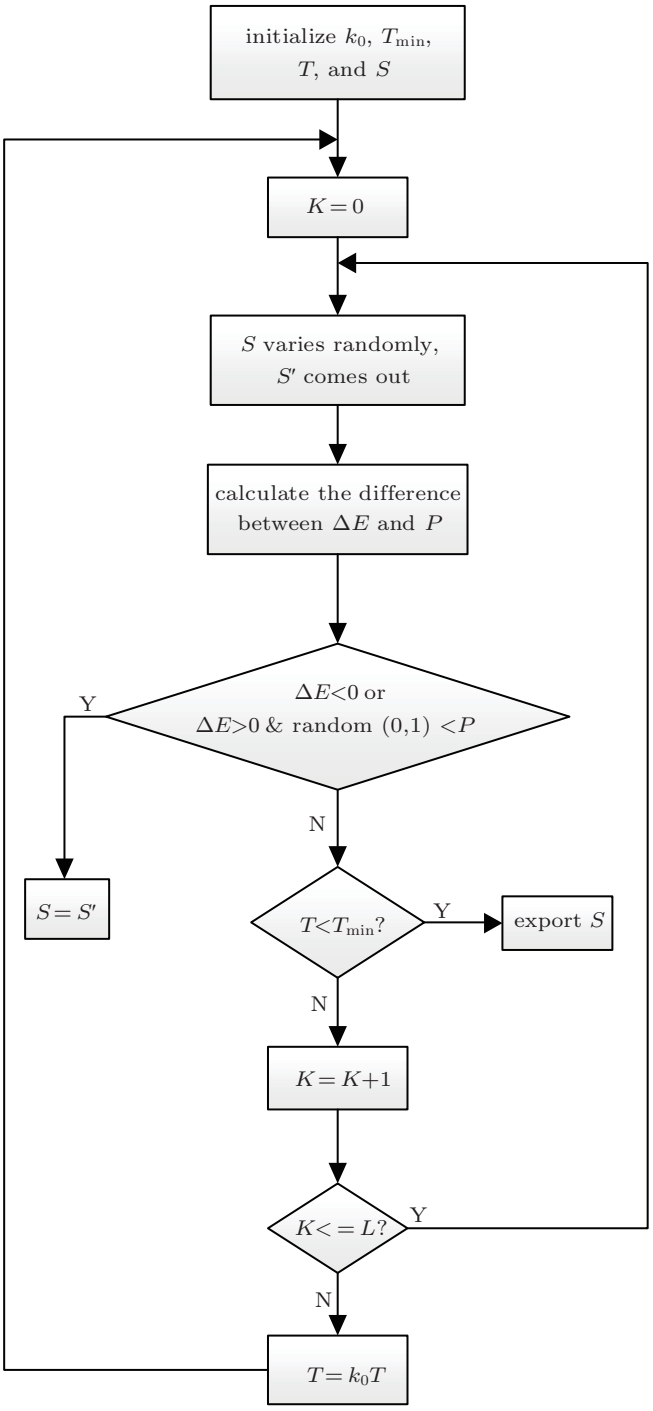


Fig. 2. Flowchart of SA.

During the annealing treatment, as the temperature decreases, the probability of accepting a worse solution gradually becomes less and less. Let L be the iteration of each temperature and $T_{\min}$ be the operation end temperature. Through repeated iterations, a new solution is generated, the energy difference is calculated. Furthermore, the resulting solution is accepted or discarded, and T is gradually reduced. When T is reduced to the value which satisfies the operator termination criterion, $T < T_{\min}$, the annealing operation ends. At the same time, the current solution is accepted as the optimization solution. The SA algorithm's flow chart is shown in Fig. 2.

3. Results and discussion

3.1. Stable structure

In order to verify the efficiency of the improved SA algorithm, the stable structures of THH Pt–Pd–Cu–Au quaternary alloy NPs with 443 atoms and 1417 atoms are studied. Figures 3(a) and 3(b) show the lowest-energy configurations of Pt–Pd–Cu–Au quaternary alloy NPs obtained by the SA algorithm. The Pt–Pd–Cu–Au quaternary atomic ratios of 0.25:0.25:0.25:0.25 are selectively illustrated in this figure to simplify the discussion. Meanwhile, the experimental results illustrate that Au and Cu tend to distribute on the surface, Pt tends to occupy the middle layers, and Pd tends to occupy the inner layers.

This stable structure of Pt–Pd–Cu–Au NPs is caused by the balance of different energies. Table 2 shows the properties of Pt, Pd, Cu, and Au. Owing to the difference of cohesive energy and surface energy, Au and Cu tend to segregate on the surface, Pt tends to distribute in the middle layers, and Pd preferentially distributes in the inner layers. This segregation will produce a lower total energy.

Table 2. Materials' properties calculated with the Q-SC potentials.[31]

Element	Atomic radius/Å	Lattice constant/Å	Cohesive energy/eV	Surface energy of [111]/J·m^{-2}
Pt	1.39	3.916	5.84	1.404
Pd	1.37	3.881	3.89	1.229
Cu	1.28	3.603	3.49	1.495
Au	1.44	4.065	3.81	0.670

Furthermore, we calculate the pair correlation function of Pt–Pd–Cu–Au quaternary alloy NPs, $N(r)$. The pair correlation function $N(r)$ is defined as the counted atom number at distance r from the center of mass. For two atom sizes (443 atoms and 1417 atoms), the atomic distribution tendencies are almost the same. Figures 3(c) and 3(d) illustrate that Au and Cu preferentially segregate on the surface, Pt tends to occupy the middle layers, while Pd tends to occupy the inner layers.

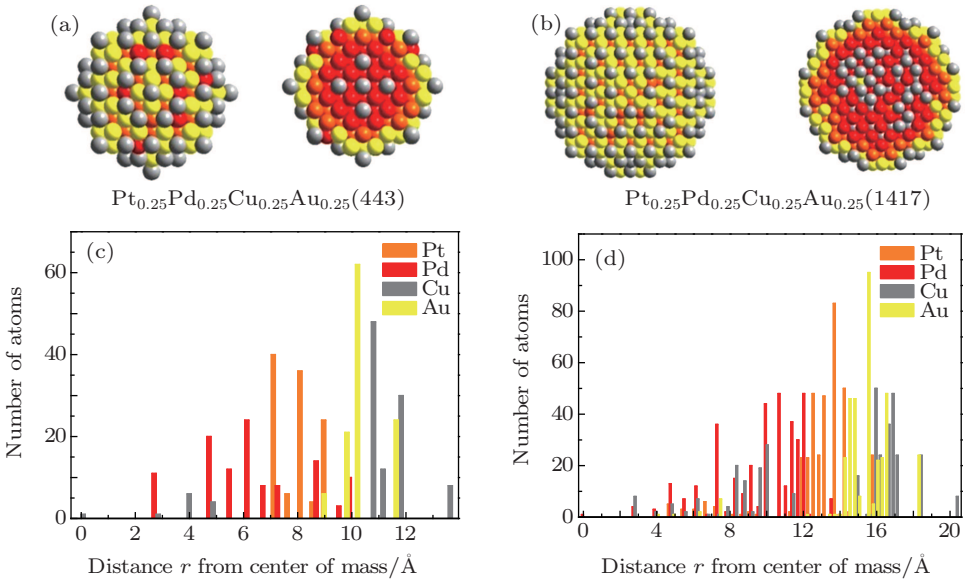


Fig. 3. (color online) Atomic configurations of Pt–Pd–Cu–Au quaternary alloy NPs with (a) 443 atoms and (b) 1417 atoms. For each pair of columns, the first and the second columns represent the whole and the cross-section atomic arrangements of the NPs, respectively. Pt atoms are in orange, Pd atoms in red, Cu atoms in gray, and Au atoms in yellow. Panels (c) and (d) show the corresponding pair correlation functions.

3.2. Core-shell distribution

The interior distribution of the Pt–Pd–Cu–Au quaternary alloy NPs with atomic ratio of 0.25:0.25:0.25:0.25 is also explored. As shown in Fig. 4, the alloy NPs are divided into several layers (a layer is also called a shell) according to the distance from the core to the atom. Evidently, there are five, seven, and nine layers in the NPs with 443 atoms, 1417 atoms, and 3285 atoms, respectively. These layers (shells) are numbered according to their distances to the center. Figure 4 shows that Au and Cu atoms tend to distribute at the outermost layers, Pt atoms tend to occupy the middle layers, and Pd atoms preferentially locate in the inner layers.

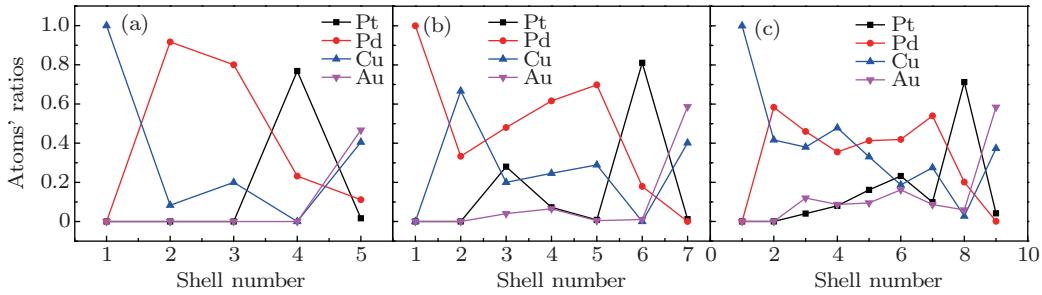


Fig. 4. (color online) Calculated atoms' ratios in each shell: (a) 443 atoms, (b) 1417 atoms, (c) 3285 atoms.

3.3. Surface segregation analysis

Noble metal NPs have broad applications in chemical and petroleum industries due to their excellent catalytic performances. Generally, chemical reactions take place on the surface, and the distribution of the atoms on the surface of multi-alloy NPs is always related to the chemical properties of the component elements. Therefore, it is vital to study Pt–Pd–Cu–Au quaternary alloy NPs' surface atomic distributions.[35]

According to Figs. 3 and 4, we have learned that Cu and Au atoms preferentially segregate to the surface. To further analyze the segregation phenomena, two cases are investigated: (i) common segregation, and (ii) competitive segregation. At the same time, we selected two NPs of 443 atoms and 1417 atoms for comparison.

Figure 5 shows Pt–Pd–Cu–Au quaternary alloy NPs' surface segregation curves when both Cu and Au compositions change from 0 to 50%. The segregation degree is measured by the surface atomic fraction, which is defined as $C = N_A/N_S$ (A is Cu or Au), where N_A is the number of surface A atoms and N_S is the number of surface atoms. In Figs. 5(a) and 5(b), the left black dotted lines represent the max segregation, while the others denote no segregation. In Fig. 5, we can see that for small amounts of Cu and Au, the Cu and Au atoms tend to segregate to the surface, and reach the max segregation. We define this segregation as the common segregation. When the

amounts of Cu and Au grow to the surface-to-volume ratio, they maintain the max segregation. With the compositions further growing, the surface Cu fraction begins to drop. We call this behavior the competitive segregation. This phenomenon is related to the lower surface energy of Au. By comparing Fig. 5(a) with Fig. 5(b), we find that the segregation degree will increase with the atomic size increasing. Herein, the surface segregation degree of Au is stronger than that of Cu with the same amounts of Cu and Au atoms. This effect is also associated with the lower surface energy of Au.

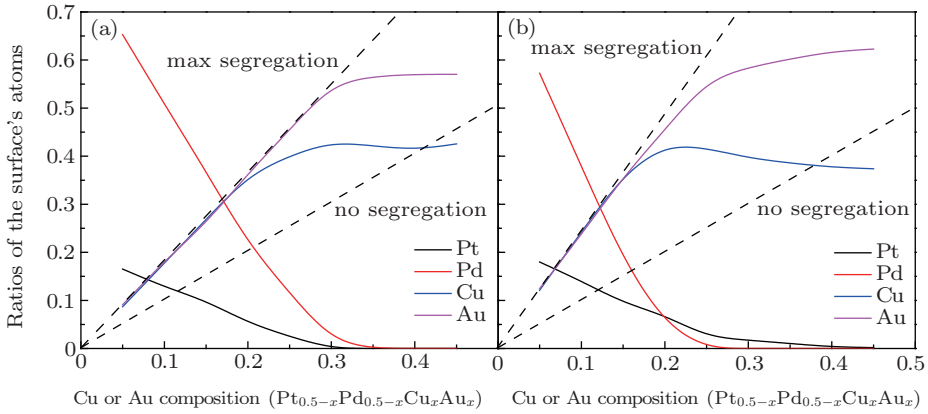


Fig. 5. (color online) Surface atomic fractions of Cu and Au with the Cu (Au) composition changing from 0 to 50% at particle sizes of (a) 443 atoms and (b) 1417 atoms.

3.4. Coordinated sites analysis

Furthermore, we investigate the preferred sites of different metal atoms. We select Pt–Pd–Cu–Au quaternary alloy NPs of 1417 atoms and analyze the preferred sites of different metal atoms (Pt, Pd, Cu and Au) by the distribution of atoms at different positions. Firstly, we change the atomic ratio of one metal; secondly, the atomic ratios of the other three metals change with the first one, and these three metals have the same atomic ratio. Figure 6 shows the concentrations of Pt and Pd atoms at different positions (different-coordinated sites), and figure 7 shows the concentrations of Cu and Au atoms at different positions (different-coordinated sites).

As shown in Figs. 6(a)–6(d), the atomic ratio of Pt increases and the atomic ratios of the other metals decrease with the increasing atomic number of Pt. It is found that the number of Pd atoms decreases most rapidly in the high coordination sites, the number of Au atoms decreases most rapidly in the middle coordination sites, whereas the number of Cu atoms decreases most rapidly in the low coordination sites.

As shown in Figs. 6(e)–6(h), the atomic ratio of Pd increases and the ratios of the other metals decrease with the increasing atomic number of Pd. It is found that, the number of Pt atoms decreases most rapidly in the high coordination sites, the number of Au atoms decreases most rapidly in the middle coordination sites, whereas the number of Cu atoms decreases most rapidly in the low coordination sites.

As shown in Figs. 7(a)–7(d), the atomic ratio of Cu increases and the atomic ratios of the other metals decrease with the increasing atomic number of Cu. It is found that, the number of Pt atoms decreases most rapidly in the high coordination sites, the number of Au atoms decreases most rapidly in the middle coordination sites, whereas the number of Pd atoms decreases most rapidly in the low coordination sites.

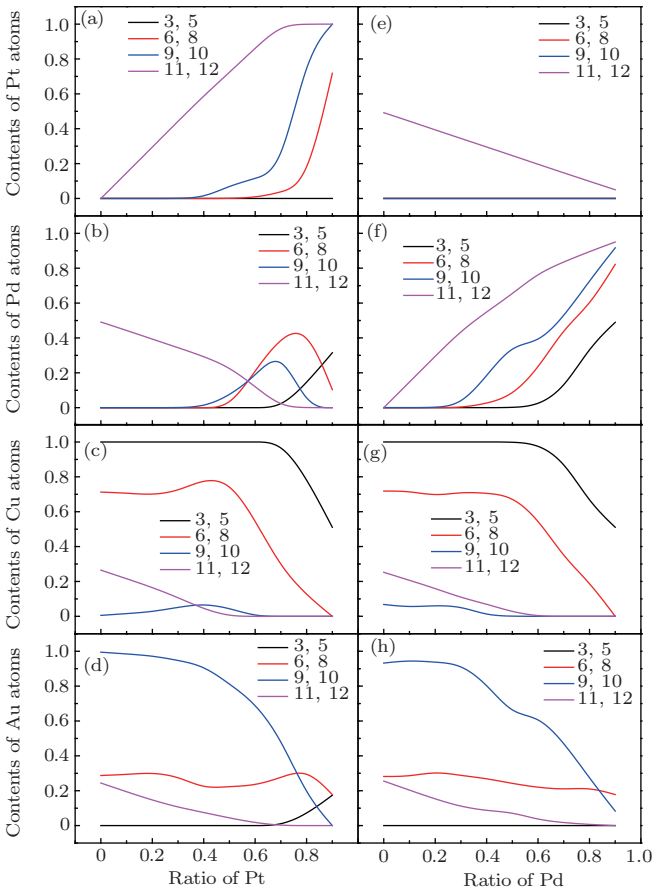


Fig. 6. (color online) Pt, Pd, Cu, and Au concentrations at different coordination sites as a function of composition of (a)–(d) Pt or (e)–(h) Pd.

As shown in Figs. 7(e)–7(h), the atomic ratio of Au increases and the ratios of the other metals decrease with the increasing atomic number of Au. It is found that, the number of Pt atoms decreases most rapidly in the high coordination sites, the number of Pd atoms decreases most rapidly in the middle coordination sites, whereas the number of Cu atoms decreases most rapidly in the low coordination sites.

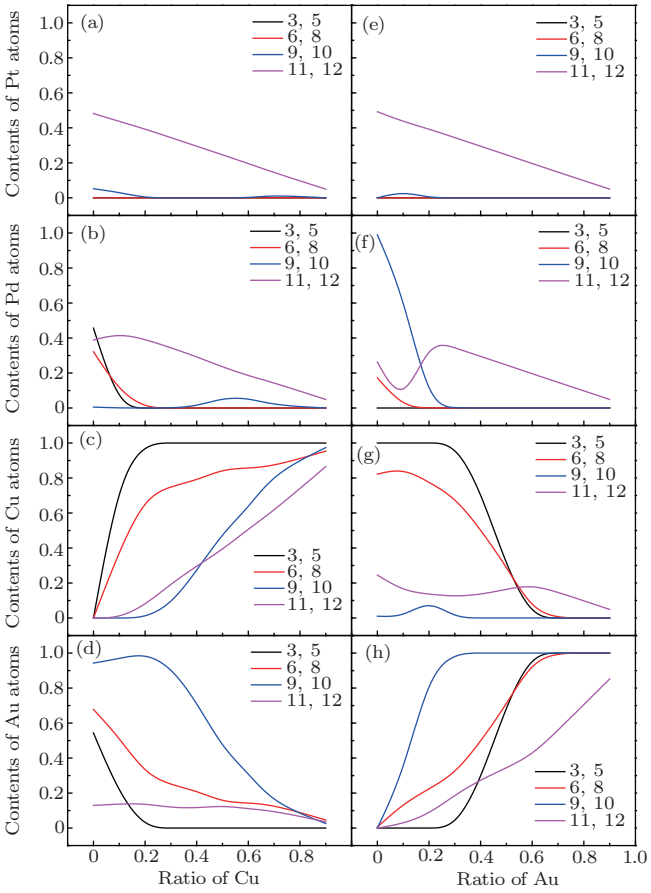


Fig. 7. (color online) Pt, Pd, Cu, and Au concentrations at different coordination sites as a function of composition of (a)–(d) Cu or (e)–(h) Au.

By comparing Fig. 6 with Fig. 7, we can find some interesting phenomena. The number of Pt atoms with the coordination numbers of 9 and 10 decreases slower than that of Pt atoms with the coordination numbers of 11 and 12. By comparison of the results in Figs. 3(c) and 3(d), we can find that the Pd atoms preferentially occupy high coordination sites (i.e., 11-fold or 12-fold coordination sites). The Pt atoms prefer to occupy the low coordination sites (9-fold or 10-fold coordination sites), the Au atoms tend to locate at middle coordination positions (6-fold or 8-fold coordination sites), and the Cu atoms tend to locate at the lowest coordination sites (3-fold or 5-fold coordination sites). The analysis of coordination number indicates that Au and Cu prefer to occupy the surface, Pt prefers to occupy the middle layers, while Pd tends to distribute in the inner layers.

4. Conclusion

We investigated the structural features and the segregation behavior of THH Pt–Pd–Cu–Au quaternary alloy NPs by using the SA algorithm. Three NPs consisting of 443 atoms, 1417 atoms, and 3285 atoms were selected to display the stable structures of the NPs. The simulated results show that Au and Cu atoms preferentially segregate to the surface, Pt atoms tend to occupy the middle layers, and Pd atoms segregate to the inner layers. With the growing particle size, the distribution of Cu atoms changes slightly. The distribution of atomic coordination number reveals that Au and Cu atoms always decrease most slowly in low coordination sites, Pd atoms decrease most slowly in high coordination sites, and Pt atoms decrease most slowly in middle coordination sites. These results are of importance not only for the experimental preparation of noble metal alloy NPs but also for further exploring the multifunctional properties of alloy NPs. Our study also confirms that the developed SA algorithm is suitable for predicting the stable structure of multimetallic NPs.

References

[1] Murray R W 2008 *Chem. Rev.* **108** 2688
[2] Zhou Z Y, Tian N, Li J T, Broadwell I and Sun SG 2011 *Chem. Soc. Rev.* **40** 4167
[3] Wu W K, Zhang L N, Ren H R, Zhang K, Li H and He Y Z 2015 *Phys. Chem. Chem. Phys.* **17** 13380
[4] Deng L, Hu W Y, Deng H Q and Xiao S F 2010 *J. Phys. Chem. C* **114** 11026
[5] Huang R, Wen Y H, Zhu Z Z and Sun S G 2012 *J. Phys. Chem. C* **116** 8664
[6] Yun K, Cho Y H, Cha P R, Lee J, Nam H S, Oh J S, Choi J H and Lee S C 2012 *Acta Mater.* **60** 4908
[7] Shao G F, Zheng W X, Tu Na Na, Liu T D and Wen Y H 2015 *Acta Phys. Sin.* **64** 013602 (in Chinese)
[8] Gao X X, Jia Y H, Li G P, Cho S J and Kim H 2011 *Chin. Phys. Lett.* **28** 033601
[9] Chen M S, Cai Y, Yan Z, Gath K K, Axnanda S and Wayne G D 2007 *Surf. Sci.* **601** 5326
[10] Pal U, Garcia-Serrano J, Casarrubias-Segura G, Koshizaki N, Sasaki T and Terahuchi S 2004 *Sol. Energ. Mat Sol. C* **81** 339
[11] Sekhon J S and Verma S S 2011 *Plasmonics* **6** 311
[12] Wang L and Yamauchi Y 2010 *J. Am. Chem. Soc.* **132** 13636
[13] Guo S J, Zhang S, Sun X L and Sun S H 2011 *J. Am. Chem. Soc.* **133** 15354
[14] Zhu L S and Zhao S J 2014 *Chin. Phys. B* **23** 063601
[15] Lumley R N, Morton A J and Polmear I J 2002 *Acta Mater.* **50** 3597
[16] Cao P, Zhang M L, Han W, Yan Y D and Chen L J 2013 *T. Nonferr. Metal. Soc.* **23** 861
[17] Mazumder V, Chi M F, More K L, and Sun S H 2010 *Angew. Chem. Int. Edit.* **49** 9368
[18] Iglesias O and Labarta A 2001 *Phys. Rev. B* **63** 184416
[19] Qin L J, Zhang Y H, Huang S P, Tian H P and Wang P 2010 *Phys. Rev. B* **82** 075413
[20] Yuge K 2010 *J. Phys.: Condens. Matter* **22** 245401
[21] Cho S H 2005 *Phys. Med. Biol.* **50** N163
[22] Guo J Y, Xu C X, Hu A M, Oakes K D and Sheng F Y 2012 *J. Phys. Chem. Solids* **73** 1350
[23] Radillo-Diaz A, Coronado Y, Péreza L A and Garzón I L 2009 *Eur. Phys. J. D* **52** 127

[24] Paz-Borbo'n L O, Guptab A and Johnston R L 2008 *J. Mater. Chem.* **18** 4154

[25] Bruma A, Ismail R, Paz-Borbón L O, Arslan H, Barcaro G, Fortunelli A, Lia Z Y and Johnston R L 2013 *Nanoscale* **5** 646

[26] Yu J M, Chen Z H, Ni Y and Li Z X 2012 *Hum. Reprod.* **27** 25

[27] Liu T D, Zheng J W, Shao G, Fan T E and Wen Y H 2015 *Chin. Phys. B* **24** 033601

[28] Wen Y H, Zhang Y, Zheng J C, Zhu Z Z and Sun S G 2009 *J. Phys. Chem. C* **113** 20611

[29] Ikeda H, Qi Y, Cagin T, Samwer K, Johnson W L and Goddard W A 1999 *Phys. Rev. Lett.* **82** 2900

[30] Sankaranarayanan S K R S, Bhethanabotla V R and Joseph B 2005 *Phys. Rev. B* **71** 195415

[31] Kimura Y, Qi Y, Cagin T and Goddard III W 1998 *Technical Report* (Vol. 3) (Pasadena: Caltech ASCI) pp. 1–29

[32] Tian N, Zhou Z Y, Sun S G, Ding Y and Wang Z L 2007 *Science* **316** 732

[33] Metropolis N, Rosenbluth A W, Rosenbluth M N and Teller A H 1953 *J. Chem. Phys.* **21** 1087

[34] Kirkpatrick S, Gelatt C D Jr. and Vecchi M P 1983 *Science* **220** 671

[35] Li Z W, Kong X S, Liu W, Liu C S and Fang Q F 2014 *Chin. Phys. B* **23** 106107